Search for neutron dark decay: $n \rightarrow \chi + e^+e^-$

X. Sun[1,a], E. Adamek[2], B. Allgeier[3], M. Blatnik[1], T.J. Bowles[4], L.J. Broussard[4], M.A.-P. Brown[3], R. Carr[1], S. Clayton[4], C. Cude-Woods[5], S. Currie[4], E.B. Dees[5,6], X. Ding[7], B.W. Filippone[1], A. García[8], P. Geltenbort[9], S. Hasan[3], K.P. Hickerson[1], J. Hoagland[5], R. Hong[8], G.E. Hogan[4], A.T. Holley[5,2], T.M. Ito[4], A. Kneckt[8], C.-Y. Liu[2], J. Liu[10], M. Makela[4], R. Mammei[11], J.W. Martin[1,11], D. Melconian[12], M.P. Mendenhall[1], S.D. Moore[5], C.L. Morris[4], S. Nepal[3], N. Nouri[3], R.W. Pattie Jr.[5,6], A.P. Galván[1], D.G. Phillips II[5], R. Picker[1], M.L. Pitt[7], B. Plaster[3], J.C. Ramsey[4], R. Rios[4,13], D.J. Salvat[8], A. Saunders[4], W. Sondheim[4], S. Sjue[4], S. Slutsky[1], C. Swank[1], G. Swift[6], E. Tatar[13], R.B. Vogelaar[7], B. VornDick[5], W. Wanchun[1], Z. Wang[4], J. Wexler[5], T. Womack[4], C. Wrede[8,14], A.R. Young[5,6], and B.A. Zeck[5]

[1] W.K. Kellogg Radiation Laboratory, California Institute of Technology, Pasadena, California 91125, USA
[2] Department of Physics, Indiana University, Bloomington, Indiana 47408, USA
[3] Department of Physics and Astronomy, University of Kentucky, Lexington, Kentucky 40506, USA
[4] Los Alamos National Laboratory, Los Alamos, New Mexico 87545, USA
[5] Department of Physics, North Carolina State University, Raleigh, North Carolina 27695, USA
[6] Triangle Universities Nuclear Laboratory, Durham, North Carolina 27708, USA
[7] Department of Physics, Virginia Tech, Blacksburg, Virginia 24061, USA
[8] Department of Physics and Center for Experimental Nuclear Physics and Astrophysics, University of Washington, Seattle, Washington 98195, USA
[9] Institut Laue-Langevin, 38042 Grenoble Cedex 9, France
[10] Department of Physics, Shanghai Jiao Tong University, Shanghai 200240, China
[11] Department of Physics, University of Winnipeg, Winnipeg, MB R3B 2E9, Canada
[12] Cyclotron Institute, Texas A&M University, College Station, Texas 77843, USA
[13] Department of Physics, Idaho State University, Pocatello, Idaho 83209, USA
[14] Department of Physics and Astronomy and National Superconducting Cyclotron Laboratory, Michigan State University, East Lansing, Michigan 48824, USA

Abstract. In January, 2018, Fornal and Grinstein proposed that a previously unobserved neutron decay branch to a dark matter particle (χ) could account for the discrepancy in the neutron lifetime observed in two different types of experiments. One of the possible final states discussed includes a single χ along with an e^+e^- pair. We use data from the UCNA (Ultracold Neutron Asymmetry) experiment to set limits on this decay channel. Coincident electron-like events are detected with $\sim 4\pi$ acceptance using a pair of detectors that observe a volume of stored Ultracold Neutrons (UCNs). We use the timing information of coincidence events to select candidate dark sector particle decays by applying a timing calibration and selecting events within a physically-forbidden timing region for conventional $n \rightarrow p + e^- + \overline{\nu_e}$ decays. The summed kinetic energy ($E_{e^+e^-}$) from such events is reconstructed and used to set limits, as a function of the χ mass, on the branching fraction for this decay channel.

1. Introduction

This paper expands on and illustrates different aspects of the analysis described in [1].

Historically, precision measurements of the neutron lifetime which use two different measurement techniques yield values that disagree at the 4σ level [2–4]. Fornal and Grinstein proposed a theoretical explanation to this neutron lifetime anomaly by suggesting a new decay channel for the neutron [5]. Instead of undergoing the conventional decay and emitting a proton with 100% branching ratio, the neutron could decay to a proton with 99% branching ratio and a dark sector particle with 1% branching ratio (see Fig. 1 for a simple description). They propose multiple cases where the dark sector particle can be accompanied by different decay products. This work uses the latest data from the Ultracold Neutron Asymmetry (UCNA) experiment to put direct constraints on one of the proposed dark decay channels: $n \rightarrow \chi + e^+e^-$, where χ is a dark sector particle.

2. Experimental apparatus

The UCNA experiment, which is located at the Los Alamos Neutron Science Center (LANSCE), has been described previously in [1,6–10]. A schematic of the apparatus is shown in Fig. 2. Here, we provide an overview of the relevant components for identifying, and constraining, a $n \rightarrow \chi + e^+e^-$ decay channel.

Neutrons, produced from a tungsten spallation target [11–13] and cooled to UCN energies (kinetic energy

[a] e-mail: xsun@caltech.edu

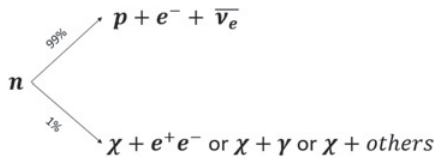

Figure 1. Simple decay diagram of the free neutron including a proposed dark decay channel. χ here represents a dark sector particle. 'Others' refer to decay channels involving a dark sector fermion [5].

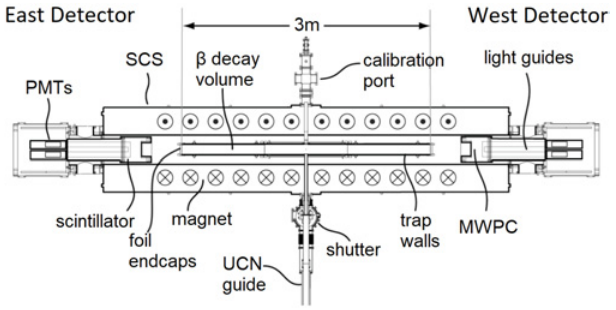

Figure 2. Schematic diagram of the UCNA experiment.

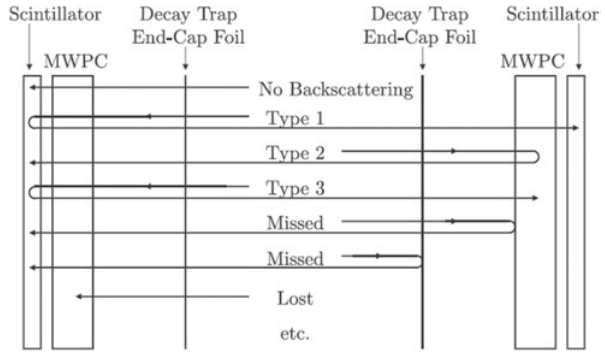

Figure 3. Schematic of potential backscattering events for a single β-decay electron [6]. Our analysis focuses on Type 1 backscatters.

<350 neV), are stored within a 3 m long decay trap in the 5 m long superconducting spectrometer (SCS). The SCS has a 1 T magnetic field which directs the decay electrons of the UCNs towards detectors located on either end [14]. We refer to these detectors as 'East' and 'West' detectors.

Each detector consists of a multiwire proportional chamber (MWPC) [15,16], followed be a 3.5 mm thick plastic scintillator. The MWPC provides position reconstruction and "backscattering" identification, i.e. electrons that scatter and do not deposit all their energy in one detector. The plastic scintillator provides energy reconstruction. The timing information is based on CAEN V775 time-to-digital converters (TDCs). In addition, in order to suppress cosmic ray backgrounds, several veto detectors are placed above, around, and behind the East and West detectors.

3. Analysis

3.1. Overview of analysis method

In attempting to detect a $n \to \chi + e^+e^-$ decay, this analysis focuses on the relative timing between triggers in the East and West detectors. In a standard $n \to p + e^- + \overline{\nu_e}$ decay, we can identify many types of events based on the

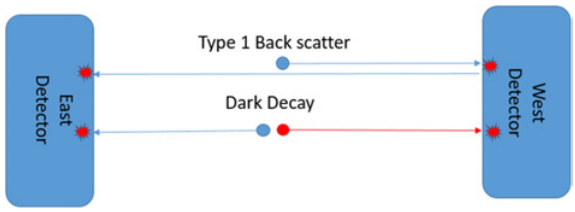

Figure 4. A diagram showing the travel paths of a proposed dark matter decay producing a e^+e^- pair, compared to a Type 1 backscatter event [17]. Both would register the same electronic signature, but there exists a lower limit on the Type 1 backscatter travel time, which is set by the maximum velocity and the crossing distance between detectors. The e^+e^- pair has no such limitations.

aforementioned backscattering. Different examples of the most common event types can be seen in Fig. 3. Due to the design of the experiment apparatus, backscatter events are suppressed, with only $\approx 3.8\%$ of events registering as coincidence events[1].

For the decay in question, $n \to \chi + e^+e^-$, the electron-positron pair can decay and travel in opposite directions towards the East and West detectors. Upon depositing all their energy, they would produce the same signature as a Type 1 single β-decay electron event, which are single β-decay electrons that deposit energy in both detectors. However, the main crux of the analysis relies on the relative timing between the two detector signals. A single backscatter event requires a minimum amount of time to traverse the spectrometer. The scintillator-to-scintillator distance is 4.4 m, which corresponds to > 16 ns travel time given the energies of our β-decay electrons. However, the electron-positron pairs can have any relative time difference since there is a probability for the decay products to register in the detectors at any time (based on different travel times from the point of decay to either detector). And hence by using the relative timing information between the two detectors, we can identify a set of events that would correspond to the $n \to \chi + e^+e^-$ decay. This argument is summarized in Fig. 4 and Fig. 5

3.2. Calibrating the time

As illustrated in Fig. 4, we expect the timing spectrum of the candidate dark matter decay events to be very different than the conventional β-decay events (see Fig. 5). Then, in principle, we just need to find the number of decay events that have a crossing time <16 ns: our "candidate dark matter" events.

The UCNA experiment uses CAEN TDCs to measure a "common-stop" signal. This means there is a large signal at a self-timing peak (STP), when an event first triggers either East or West detector, and subsequently starts the TDC. If the decay is a multi-trigger event, then there will be a timing spectrum that represents the difference between the first trigger registered in either detector and the second trigger, registered in the opposite detector. A sample TDC spectrum is shown in Figure 6. A conversion from channels to time is given by the electronics.

[1] In this paper, coincidence events refer to events that deposit energy above threshold in both the East/West scintillator and wirechamber.

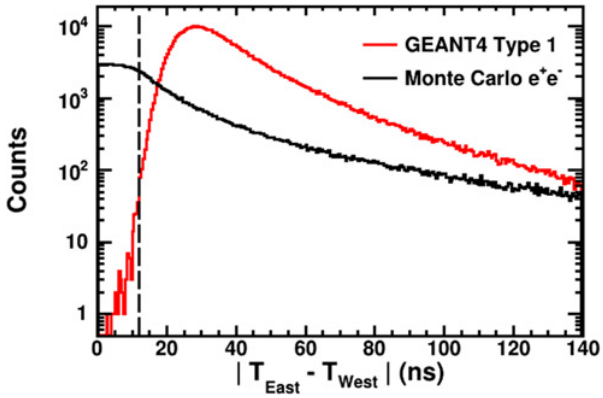

Figure 5. A simulated timing spectrum of a Type 1 decay event (red) vs. a e^+e^- dark matter decay event (black), assuming a 1% branching ratio for the dark matter decay. The timing spectrum is generated by sampling a simple three-body phase space for the χ, e^+, e^- and assuming the maximum available summed kinetic energy, 644 keV, for the e^+e^- pair. The dotted line represents the chosen timing window for this analysis. Bin width of 50 ps.

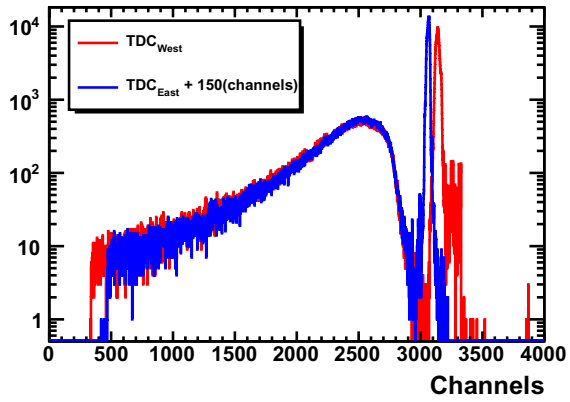

Figure 6. Shows the measured TDC response in the West (red) and East (blue) detectors. A flat channel shift is applied to the East detector which aligns the Type 1 backscatter peak with that of the West detector. A channel-to-time conversion is applied by setting the self-timing peak channel center to 140 ns, i.e. the electronics setting. After conversion, the Type 1 backscatter peak matches the GEANT4 Monte Carlo. Note that there is a channel offset between the East and West self-timing peaks. This is attributed to additional dead-time in the West detector due to cable length differences. Bin width of ≈50 ps.

Due to electronic jitter, once the TDC data was calibrated to a physical time, there was ≈ 4 ns spread in the East, West STPs. This gave a rough estimate of the timing error of 2 ns. Furthermore, there was an unphysical "dead-time" included in the timing measurement due to differences in cable lengths (and hence transit times for the hardware triggers). This was calibrated using the full, Type 1, β-decay timing spectrum. By aligning the TDC spectra of the two detectors at the Type 1 backscatter peak (≈ 2600 channels, Fig. 6), we identify that the TDC West detector timing window starts ≈ 1.7 ns after the TDC East detector, based on the channel differences between the STPs. We cut this unphysical dead-time from the analysis window.

Next we compare with a full GEANT4 Monte Carlo simulation of the Type 1 events timing spectra [8,18].[2] After background-subtracting, and including

[2] The GEANT4 framework is described in more detail in [19].

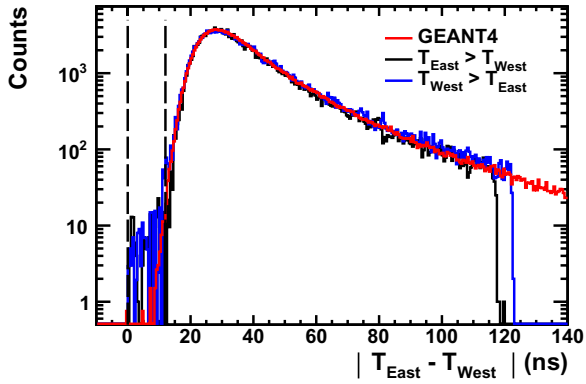

Figure 7. Shows the background-subtracted, relative time differences between events that first trigger the East detector (blue) and events that first trigger the West detector (black). An overlaid GEANT4 simulation (red) shows the expected timing spectrum for conventional β-decay Type 1 backscatter events. Dotted lines illustrate the chosen time window used in this analysis to identify candidate dark matter decays. Bin width of 50 ps.

scaling for differences in live-time between background and foreground runs[3], we find good agreement between the GEANT4 simulated timing spectra [8] and our measured Type 1 timing spectra, see Fig. 7.

This validates our timing calibration and allows us to set physical timing window cuts that correspond to candidate dark matter decays.

3.3. Efficiencies

There are three main "loss" methods when considering the total efficiency of the detectors: kinematics, trigger probability, and timing window cuts.

First, the kinematic losses refer to neutron β-decays that produce a e^+e^- pair that travel in the same direction. These events are rejected because they would not produce the timing signature that we use to greatly reduce background from the standard neutron β-decay: $n \rightarrow pe^-\overline{\nu_e}$. We estimate this effect using a toy Monte Carlo simulation which samples the available phase space from a standard three-body decay, $\chi + e^+e^-$, and selects oppositely-directed e^+e^-. This loss corresponds to ≈ 60% of all β-decays when integrated over the allowed values of m_χ.

Second, the trigger probability refers to the probability that an electron at a particular energy will be detected by our apparatus. In the UCNA experiment, the trigger probability has been characterized extensively in [7,8,18]. In addition, a reduction must be applied since there is a lower probability of capturing the full energy of a positron compared to an electron. A full GEANT4 simulation of our detector shows that the fraction of positrons that deposit their full energy in our detectors compared to an electron is ≈ 15% smaller, primarily due to escaping annihilation gammas. The trigger function inefficiency, estimated at a conservative 20%, would reduce the acceptance by a negligible amount at high summed kinetic energies (i.e. a 2% effect at 644 keV). At lower energies, it rises:

[3] The experiment was optimized for the measurement of the A asymmetry parameter [7] and hence the live-time of foreground to background was 5:1. For this analysis, this live-time difference means the background runs dominate our errors.

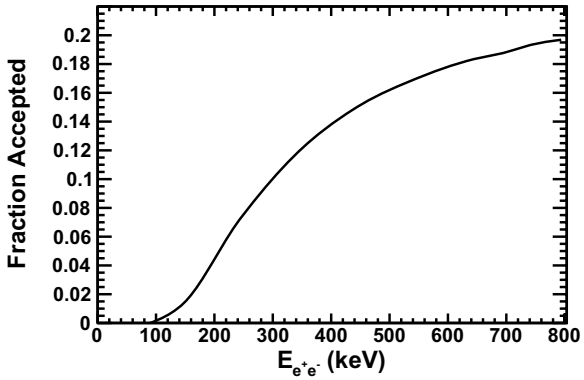

Figure 8. The total acceptance of our detector to e^+e^- pair particles, given as a fraction of accepted events, over the available energy range of the produced pair. This folds together the kinematic, trigger, and timing window cut efficiencies.

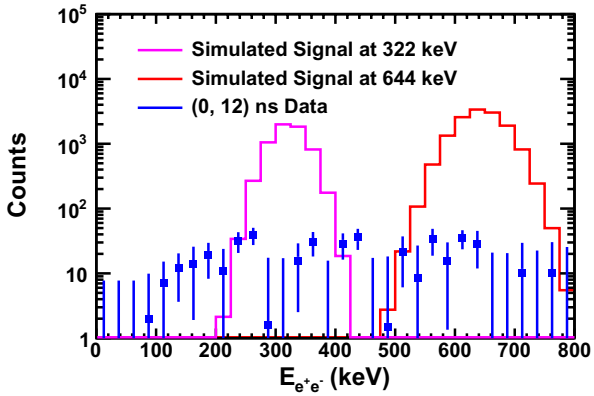

Figure 9. Background-subtracted e^+e^- pair kinetic energy spectra for events in our analysis time window (blue). For comparison, simulated positive dark matter decay signals at 322 keV (purple) and 644 keV (red) are overlaid.

becoming 8% at 244 keV, and increasing to 60% at 144 keV.

Third, our timing window cut changes the acceptance probability of our candidate dark matter decay events. Candidate dark matter decays to e^+e^- will arrive at the two detectors with a range of time differences due to differences in pitch angle, relative distances to the two detectors, differences in initial energy and momentum, and so on. A shorter time window would reduce our acceptance probability, but a longer time window introduces significant background contamination of conventional β-decay Type 1 events. Given previous discussions, and further analysis into valid time windows, a timing window was chosen from 0 to 12 ns. The corresponding acceptance probability ranges from $\approx$ 20–40% over the range of allowed $E_{e^+e^-}$. Examining neighboring "bins" of ± 2 ns in a timing Monte Carlo, across several χ masses, gives an uncertainty of approximately 15% in the timing window acceptance.

We get the total efficiency of the detector by multiplying these three effects together. The result can be seen in Fig. 8.

3.4. "Look-elsewhere" Effect

Final exclusion confidence limits are determined using the background-subtracted dataset, shown in Fig. 9, binned into discrete energy bins with width comparable to the energy resolution, and checked for bin aliasing. Since we are searching for a peak structure over a range of energies, fluctuations at other energies must be considered. This is usually termed the "look-elsewhere effect" - the probability that a statistically significant fluctuation will occur given enough samples [20].

This look-elsewhere effect was accounted for numerically, drawing on the method used in [21]. First, a statistical test was constructed,

$$\xi = \sum_i \frac{N_i - \mu_i}{\sigma_i} \text{ for } N_i > \mu_i \qquad (1)$$

where N_i is a normally-distributed random variable for bin i with mean μ_i and standard deviation σ_i, and both μ_i and σ_i are given by the data. ξ is computed with a large number of Monte Carlo samples for each final energy bin, as well as the "single-bin" dataset, i.e. when all events are considered together. The ratio of the single-bin ξ distribution to the ξ_i distributions provides the look-elsewhere correction factor.[4] This correction is applied to the cumulative distribution function (CDF) of the single-bin confidence levels. The corresponding CDF for the individual energy bins is solved for numerically to obtain new confidence levels, giving us our final confidence limits.

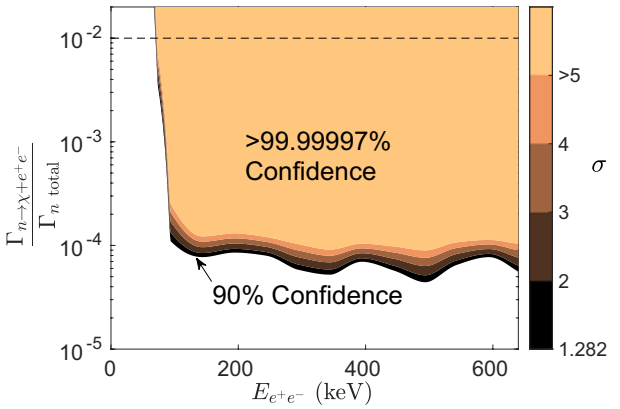

Figure 10. Confidence limits on the branching ratio of the neutron dark decay channel, as a function of the kinetic energy of the produced e^+e^- pair. This is directly related to the proposed χ mass by $m_\chi = m_n - 2m_e - E_{e^+e^-}$, which has a range of 937.900 MeV $< m_\chi <$ 938.543 MeV. A branching ratio of 10^{-2}, which would be required to explain the neutron lifetime anomaly if $n \to \chi + e^+e^-$ were the only allowed final state, is shown by the dashed line.

4. Final Confidence Limits

After calibrating the timing spectrum, applying event type and timing window cuts, correcting for total acceptance, and correcting for the look-elsewhere effect, we get the final confidence limits shown in Fig. 10.

Assuming the neutron dark matter decay channel, $n \to \chi + e^+e^-$, exists at the 1% level necessary to resolve the neutron lifetime anomaly, we exclude this decay channel at $\gg 5\,\sigma$ for summed kinetic energy $E_{e^+e^-} > 100$ keV. If it is not the only decay channel, we set a branching ratio limit

[4] Also known as the "trials factor".

$\Gamma_{n\to\chi+e^+e^-}/\Gamma_{n\ \mathrm{total}} < 10^{-4}$ at the 90% confidence level, over the same energy range of $E_{e^+e^-} > 100\,\mathrm{keV}$.

5. Further discussion

This analysis, expanding upon [1], investigates Fornal and Grinstein's proposal of a neutron dark matter decay [5] explanation of the neutron lifetime anomaly [2–4].

We take advantage of an old dataset that was originally optimized to measure the asymmetry parameter of the free neutron, "A", in order to set limits on candidate dark matter decays. Better characterization of the timing window cuts, the fidelity of the TDC self-timing peak calibration, and incorporating the 2011–2012 dataset (which would require far greater work in calibrating because the TDCs were less stable during the 2011–2012 run) might improve the confidence limits by a factor between 2 and 5. However, given that this analysis already rules out the proposed decay channel (presuming that it is the only dark matter decay channel) as an explanation of the neutron lifetime anomaly at $\gg 5\,\sigma$, we do not anticipate further work on this dataset.

This work is supported in part by the US Department of Energy, Office of Nuclear Physics (DE-FG02-08ER41557, DE-SC0014622, DE-FG02-97ER41042) and the National Science Foundation (1002814, 1005233, 1205977, 1306997, 1307426, 1506459, and 1615153). We gratefully acknowledge the support of the LDRD program (20110043DR), the AOT division of the Los Alamos National Laboratory, and helpful discussions with B. Grinstein.

References

[1] X. Sun et al. (UCNA Collaboration), Phys. Rev. C **97**, 052501 (2018)
[2] G.L. Greene, P. Geltenbort, Sci. Am. **314**, 37 (2016)
[3] F.E. Wietfeldt, G.L. Greene, Rev. Mod. Phys. **83**, 1173 (2011)
[4] A.R. Young et al., J. Phys. G **41**, 114007 (2014)
[5] B. Fornal, B. Grinstein, Phys. Rev. Lett. **120**, 191801 (2018)
[6] B. Plaster et al. (UCNA Collaboration), Phys. Rev. C **86**, 055501 (2012)
[7] M.P. Mendenhall et al. (UCNA Collaboration), Phys. Rev. C **87**, 032501 (2013)
[8] M.A.P. Brown, E.B. Dees et al. (UCNA Collaboration), Phys. Rev. C **97**, 035505 (2018)
[9] K.P. Hickerson et al., Phys. Rev. C **96**, 042501 (2017), [Addendum: Phys. Rev. C96, no.5, 059901(2017)], 1707.00776
[10] A.T. Holley et al., Rev. Sci. Instrum. **83**, 073505 (2012), https://doi.org/10.1063/1.4732822
[11] A. Saunders et al., Phys. Lett. B **593**, 55 (2004)
[12] C. Morris et al., Phys. Rev. Lett. **89**, 272501 (2002)
[13] A. Saunders et al., Rev. Sci. Instrum. **84**, 013304 (2013), https://doi.org/10.1063/1.4770063
[14] B. Plaster et al., Nucl. Instrum. Meth. A **595**, 587 (2008), 0806.2097
[15] T.M. Ito et al., Nucl. Instrum. Meth. A **571**, 676 (2007), physics/0702085
[16] C.L. Morris et al., Nucl. Instrum. Meth. A **599**, 248 (2009)
[17] C. Swank (2018), talk at the Conference on the Intersections of Particle and Nuclear Physics. http://cipanp18.berkeley.edu/
[18] M. Mendenhall, Ph.D. thesis, California Institute of Technology (2014)
[19] S. Agostinelli et al. (GEANT4), Nucl. Instrum. Meth. A **A506**, 250 (2003)
[20] L. Lyons, Ann. Appl. Stat. **2**, 887 (2008)
[21] F. Beaujean, A. Caldwell, O. Reimann, Eur. Phys. J. C **78**, 793 (2018), 1710.06642